JLA *Journal of Lipid and Atherosclerosis*

Original Article

Check for updates

Chylomicron Characteristics Are Associated With Microsomal Triglyceride Transfer Protein in an Animal Model of Diet-Induced Dysbiosis

Carolina Olano [iD],[1,2] Gregorio Fariña [iD],[1,2] Morena Wiszniewski [iD],[3]
Jimena Medel [iD],[4] Celina Morales [iD],[4] Silvia Friedman [iD],[5] Vanesa Macri [iD],[5]
Magalí Barchuk [iD],[1,2,6] Gabriela Berg [iD],[1,2,6] Laura Schreier [iD],[1,2] Valeria Zago [iD] [1,2,6]

[1]Laboratorio de Lípidos y Aterosclerosis, Departamento de Bioquímica Clínica, Facultad de Farmacia y Bioquímica, Universidad de Buenos Aires, Buenos Aires, Argentina
[2]Instituto de Fisiopatología y Bioquímica Clínica (INFIBIOC), Facultad de Farmacia y Bioquímica, Universidad de Buenos Aires, Buenos Aires, Argentina
[3]CONICET – Universidad de Buenos Aires, Centro de Estudios Farmacológicos y Botánicos (CEFyBO), Facultad de Medicina, Universidad de Buenos Aires, Buenos Aires, Argentina
[4]Departamento de Patología, Instituto de Fisiopatología Cardiovascular, Facultad de Medicina, Universidad de Buenos Aires, Buenos Aires, Argentina
[5]Cátedra de Bioquímica General y Bucal, Facultad de Odontología, Universidad de Buenos Aires, Buenos Aires, Argentina
[6]CONICET, Facultad de Farmacia y Bioquímica, Universidad de Buenos Aires, Buenos Aires, Argentina

ORCID iDs
Carolina Olano [iD]
https://orcid.org/0009-0005-0742-867X
Gregorio Fariña [iD]
https://orcid.org/0009-0006-7707-3912
Morena Wiszniewski [iD]
https://orcid.org/0000-0003-2191-981X
Jimena Medel [iD]
https://orcid.org/0009-0007-6597-6572
Celina Morales [iD]
https://orcid.org/0009-0006-7276-8344
Silvia Friedman [iD]
https://orcid.org/0000-0003-4666-9036
Vanesa Macri [iD]
https://orcid.org/0000-0001-8084-5676

ABSTRACT

Objective: Intestinal remnant chylomicrons (CMs) are involved in cardiovascular residual risk and the atherogenic process. Microsomal triglyceride transfer protein (MTTP) catalyzes the assembly of lipids to apolipoprotein B48, generating CMs. Dysbiosis could alter this behavior. This study investigated the chemical composition of CMs and their associations with intestinal MTTP and gut fat depots in a diet-induced dysbiosis animal model.
Methods: Male Wistar rats were fed either a standard diet (control, n=10) or a high-fat high-sucrose diet (HFSD, n=10) for 14 weeks. Measurements included serum glucose, lipid-lipoprotein profile, free fatty acids (FFAs), lipopolysaccharide (LPS) and the *Firmicutes/Bacteroidetes* (F/B) ratio in stool samples, via real-time quantitative polymerase chain reaction. Lipid content in isolated CMs (ultracentrifugation d <0.95 g/mL) was assessed, and MTTP, cell intestinal fat content (CIF), histology, apoB mRNA and tight junction (TJ) proteins were analyzed, in intestinal tissue.
Results: Compared to control, HFSD rats showed higher levels of LPS, triglycerides (TGs), non-high-density lipoprotein cholesterol (HDL-C) levels, TG/HDL-C ratio, FFAs, and the F/B ratio. HFSD CMs showed increased TG and phospholipids. TJ proteins levels were lower in the HFSD group, while histological scores showed no differences. CIF was increased in the HFSD group. No significant differences in apoB mRNA were found. MTTP expression was higher in the HFSD group, and directly correlated with CM-TG and inversely correlated with CIF.
Conclusion: Our findings imply that gut TG content may constitute an important determinant of the secretion of TG-rich CMs, promoted by MTTP, with increased atherogenic potential.

Keywords: Chylomicrons; Dysbiosis; MTTP; Atherogenic risk; Triglycerides

Magalí Barchuk [ID]
https://orcid.org/0000-0001-6454-9869
Gabriela Berg [ID]
https://orcid.org/0000-0002-5787-8960
Laura Schreier [ID]
https://orcid.org/0000-0002-6973-055X
Valeria Zago [ID]
https://orcid.org/0000-0002-1083-4346

INTRODUCTION

Chylomicrons (CMs) are large, triglyceride (TG)-rich lipoproteins produced by intestinal enterocytes in response to fat ingestion. Their primary function is to transport dietary lipids to various tissues for storage or energy use. The degradation products of TG hydrolysis by lipoprotein lipase (LPL) are known as remnant CMs (rCMs).[1,2] It has been suggested that rCMs, along with very low-density lipoprotein (VLDL) remnants, play a significant role in cardiovascular residual risk and contribute to the atherogenic process. Although CM particles are too large to penetrate the vessel wall, rCM particles are sufficiently small to enter the subendothelial space and contribute to the formation of atherosclerotic lesions.[3] Given the high affinity of LPL for CMs, it is expected that TG-over-enriched CMs would be more efficiently hydrolyzed by LPL, resulting in the formation of smaller particles with atherogenic potential.

Increased intestinal CM and rCM production is commonly observed in conditions with high prevalence such as obesity, type 2 diabetes, and other insulin resistance (IR) states. These particles, along with hepatic VLDL and its remnants, contribute to the postprandial hypertriglyceridemia seen in these diseases.[4,5] In previous studies involving both animal models and patients with IR, we have shown that qualitative changes in VLDL are linked to endothelial dysfunction, which in turn increases the cardiovascular risk associated with IR.[6,7]

The gut is inhabited by a diverse community of microorganisms known as the gut microbiota (GM), which includes approximately 100 trillion bacteria.[8] An imbalance in the GM, often referred to as dysbiosis, is increasingly recognized as a significant cardiometabolic risk factor in diseases related to IR states. Dietary changes significantly impact the composition and function of the GM, potentially leading to the development of an atherogenic metabolic profile.[9,10] Furthermore, it has been established that a high-fat, high-sucrose diet (HFSD) alters the GM composition. This diet reduces the prevalence of specific bacteria that protect the gut barrier while increasing the prevalence of opportunistic pathogens. The *Firmicutes*/*Bacteroidetes* (F/B) ratio serves as a marker for microbiota dynamics and has been well validated in both rodent and human studies.[11]

There is a proximal to distal permeability gradient that regulates the paracellular transport of substances through tight junction (TJ) transmembrane proteins, which are essential for maintaining intestinal integrity. Alterations in these proteins can lead to barrier dysfunction and elevated plasma levels of endotoxins such as lipopolysaccharides (LPS), potentially resulting in the development of metabolic disorders.[12-14] However, the metabolic alterations associated with intestinal dysbiosis induced by an HFSD, particularly concerning CMs, have not been extensively studied.

CM synthesis is a complex process involving multiple steps, with apolipoprotein B48 (apoB48) and microsomal triglyceride transfer protein (MTTP) playing crucial roles. ApoB48, a spliced product of the apoB100 gene specific to the intestine and a primary non-exchangeable protein, serves as the structural backbone of CM. Each mature CM particle contains a single molecule of apoB48[15]; thus, measuring its levels provides an indication of the particle count of this lipoprotein.

MTTP plays a crucial role in CM synthesis as it primarily catalyzes the assembly of TG, cholesterol ester, and phospholipids into apoB48, thereby producing primordial CM. Alterations in MTTP expression or activity can lead to the formation of modified CM

particles, which disrupt normal catabolism and promote the accumulation of TG in intestinal ectopic stores. A reduction in intestinal MTTP expression, whether due to genetic mutations or targeted disruptions in animal models, has been shown to decrease CM production by 80%, and is associated with varying degrees of intestinal steatosis.[16-18] In contrast, conditions such as IR or a high-fat diet (HFD) promote the expression of this protein, thereby increasing the synthesis and secretion of intestinal lipoproteins. Although limited research has been conducted on the role of intestinal MTTP in dysbiosis,[19] there are currently no studies exploring the relationship between intestinal MTTP and the lipid composition of synthesized CMs, beyond their serum levels. Additionally, it remains unclear whether altered microbiota environments in intestinal fat depots influence the TG content of CM particles.

In this context, our aim was to evaluate the chemical characteristics of CMs and their association with intestinal MTTP expression, as well as their relationship with intestinal fat depots in a diet-induced dysbiosis animal model.

MATERIALS AND METHODS

1. Animals and diet

Male Wistar rats (n=20) obtained from the animal laboratory at the Cátedra de Bioquímica General y Bucal, Facultad de Odontología, Universidad de Buenos Aires (Argentina), were housed under controlled conditions with temperatures maintained at 20°C–22°C, humidity levels at 50%–60%, and consistent airflow. A fixed 12-hour light/dark cycle was also established. All experimental procedures adhered to the National Institute of Health Guide for the Care and Use of Laboratory Animals. The protocol received approval from the Comité Institucional para el Cuidado y Uso de Animales de Laboratorio at the Facultad de Farmacia y Bioquímica, Universidad de Buenos Aires (Argentina.REDEC-2020-2292-E-UBA-DCT-FFYB).

Until the start of the experiment, all animals were fed a standard laboratory chow diet for rats, ensuring unrestricted access to both food and water to standardize their nutritional status. This diet provided approximately 2.17 kcal/g of chow. Once the rats reached a weight of 180–220 g, they were randomly assigned to one of two groups: experimental or control. The experimental group (HFSD, n=10) received a HFD and 15% sucrose solution in their drinking water, while the control group (n=10) continued on the chow diet for the duration of the 14-week study. For the preparation of the HFD, standard rodent chow pellets were ground into powder and mixed with a fat source—lard and high oleic sunflower oil—making up 40% of the total caloric content (15% of which was saturated fat), and then repelleted. The HFSD provided 286 kcal per 100 g. Chow was prepared weekly under sterile conditions, packaged in individual plastic sealed bags containing enough food for one day, and stored at −20°C. Any remaining chow was discarded daily. Body weight and caloric intake were monitored weekly throughout the experimental period. Additionally, any signs of dehydration in the animals were assessed by measuring plasma sodium levels.

2. Samples

After 14 weeks of treatment, food and water were withheld at the end of the dark period, which was at 7:00 AM. To minimize fasting time and ensure the presence of rCMs, animals were sacrificed over two days, with groups alternated accordingly. Each animal was weighed and then anesthetized using an intraperitoneal injection of sodium pentothal (60 mg/kg body weight). Blood samples were collected via cardiac puncture under aseptic conditions. The

serum was isolated and maintained at 4°C for up to 24 hours for glucose and lipid-lipoprotein profiling, or it was frozen at −70°C for subsequent CM, free fatty acid (FFA), and LPS analysis. Stool samples were taken from the distal colon and immediately frozen at −70°C for F/B ratio assessment using quantitative polymer chain reaction (qPCR) analysis.

Segments of the duodenum were flash-frozen in liquid nitrogen and stored at −80°C for western blotting, real-time qPCR (RT-qPCR), and fat content assessments. Other pieces of the duodenum, jejunum, and ileum were fixed in a 10% formalin buffer at pH 7.0 and preserved at 4°C for histological evaluation. Intestinal, epididymal, and perirenal adipose tissues were weighed to assess total body fat content. Epididymal adipose tissue was utilized as a representative of visceral adipose tissue (VAT).

3. Biochemical measurements

Serum glucose, total cholesterol, and TG were measured using commercial enzymatic kits, while high-density lipoprotein cholesterol (HDL-C) was assessed through a standardized homogeneous method (Roche) on a Cobas C-501 autoanalyzer. The intra-assay coefficient of variation (CV) was less than 1.9%, and the interassay CV was less than 2.4% for all parameters. To evaluate atherogenic lipoproteins, non-HDL-C was calculated by subtracting HDL-C from total cholesterol. The TG/HDL-C index was used as a surrogate marker of IR. FFA levels were determined using an enzymatic colorimetric method (Randox). LPS levels were measured using the Pierce LAL chromogenic endotoxin quantitation kit (Thermo Fisher Scientific; Invitrogen). To prevent contamination with exogenous LPS, extreme care was taken by utilizing single-use nonpyrogenic supplies and pyrogen-free pipette tips.

4. Isolation and lipid composition of the CM-rich fraction

CM-rich fractions were isolated using preparative ultracentrifugation. This involved diluting the serum sample by half with pyrogen-free water to achieve a density of less than 0.95 g/mL. The process was carried out in a Beckman XL-90 ultracentrifuge, utilizing a fixed angle rotor type 90 Ti. Each centrifugation run was conducted at $16,155 \times g$ (17,000 rpm) for 15 minutes at 15°C. The purity of the lipoprotein fraction was assessed through agarose gel electrophoresis.

Isolated CM-cholesterol and TG were assessed using previously described methods, while CM-PL levels were determined by the Fiske-Subbarow method.[20] Data were expressed in mg/dL for each isolated lipoprotein fraction.

5. Measurements of intestinal fat content

Intestinal lipid content was assessed using a Folch extraction, followed by evaporation to dryness and gravimetric measurement. Pieces of the gut were weighed, moisturized, and homogenized with 1.5 mL of methanol. A 200 μL aliquot of the methanol homogenate was then combined with 400 μL of chloroform and 100 μL of water. Each sample was analyzed in duplicate. Following incubation at 4°C, the samples were centrifuged at the same temperature for 10 minutes at 10,000 rpm. The organic phase was subsequently collected and evaporated under a stream of N_2 gas. Cell intestinal fat (CIF) content was quantified as grams per gram of total tissue.[21]

6. ApoB assessed by RT-qPCR

ApoB total RNA was extracted from 50 mg of jejunum tissue using Quickzol reagent (Kalium Technologies), following the manufacturer's instructions. Reverse transcription was conducted using MMLV reverse transcriptase (Thermo Fisher Scientific). The qPCR

amplifications were performed on a Rotor-Gene 6000 Corbett Life Science Real Time Thermal Cycler (Corbett Research) and the results were quantified using Rotor Gene 6000 Series Software (version 1.7 Build 40).[22] The primer oligonucleotide sequences used in this study were:

ApoB forward: 5′-AGTAGTGGTGCGTCTTGGATCCA-3′
ApoB reverse: 5′-ACTCTGCAGCAAGCTGTTGAATGT-3′
18s forward: 5′ ACGGAAGGGCACCACCAGGA 3′
18s reverse: 5′ CACCACCACCCACGGAATCG 3′

Gene expression levels were normalized to 18s ribosomal RNA, serving as an internal control, through the efficiency-calibrated method for relative quantification.[23]

7. MTTP expression by western blotting

Duodenum tissue was homogenized in 250 mM sucrose, 50 mM Tris buffer (pH 7.4), and 2% protease inhibitor cocktail (Sigma Aldrich). The homogenates were then centrifuged at 10,000 rpm and 4°C for 10 minutes. The resulting supernatant was utilized for protein determination using Lowry's method.[24] For the detection of MTTP (99 kDa) and β-actin (42 kDa), 50 μg of protein or 2 μL of pre-stained molecular weight standards (BioRad) were loaded onto a 10% SDS-PAGE gel. Subsequently, the gels were electroblotted onto a polyvinylidene difluoride membrane. The membranes were blocked with 5% powdered skim milk for 1 hour and then probed overnight at 4°C with a rabbit polyclonal IgG antibody to the MTTP C-terminal (Abcam; 1/300) or an antibody to β-actin (Sigma Aldrich, 1/300). After washing with Tris-buffered saline containing 0.1% Tween, the blots were incubated with an HRP-conjugated secondary antibody to rabbit (BioRad) for 90 minutes at room temperature. The blots were then scanned and quantified using a C-Digit scanner (Li-Cor Biosciences). Results are expressed as the ratio of MTTP protein to β-actin protein (relative units, RU).

8. Intestinal integrity evaluation by RT-qPCR

For the characterization of TJ transmembrane proteins, total RNA was extracted from 50 mg of ileum tissue using Quickzol reagent (Kalium Technologies), following the manufacturer's instructions. RNA quantification and quantitative real-time PCR were conducted as outlined in section 2.6 for apoB. The primer oligonucleotide sequences used in this study were:

Zonula occludens-1 forward: 5′ CCATCTTTGGACCGATTGCTG 3′
Zonula occludens-1 reverse: 5′ TAATGCCCGAGCTCCGATG 3′
Claudin forward: 5′ CCTGGCTGAGACTCCATCAC 3′
Claudin reverse: 5′ CGAAGCCAGGATGAAACCCA 3′
Occludin forward: 5′ CCTTTTGCTTCATCGTTCCTTG 3′
Occludin reverse: 5′ AGTCGGGTTGACTCCCATTAT 3′
18s forward: 5′ ACGGAAGGGCACCACCAGGA 3′
18s reverse: 5′ CACCACCACCCACGGAATCG 3′

Gene expression levels were normalized to 18s ribosomal RNA as an internal control, using the efficiency-calibrated method for relative quantification.[23]

9. Characterization of dysbiosis by qPCR

Bacterial DNA was extracted from stool colon samples using the High Pure PCR template preparation kit (Roche Diagnostics). Each specific bacterial phylum was identified

through RT-PCR. For this purpose, specific primers were synthesized and compared with a curated database of bacterial 16S RNA (SILVA). PCR conditions were optimized to ensure specific amplification using standard bacterial strains: *Enterococcus faecalis* ATCC 29212 as a representative of *Firmicutes*; *Bacteroides fragilis* ATCC 25285 as a representative of *Bacteroidetes*; and *Escherichia coli* ATCC 25922 as a representative of the total bacterial population (*Eubacteria*).

These bacterial strains were also utilized to construct a calibration curve based on the quantification of genomic DNA, which was measured by the sample's absorbance at 260 nm. The results were expressed as the F/B ratio, normalized to the total bacterial DNA content in the samples. The specific primers used were:

> *Firmicutes* forward 5′ GGAGTATGTGGTTTAATTCGAAGCA 3′
> *Firmicutes* reverse: 5′ AGCTGACGACAACCATGCAC 3′
> *Bacteroidetes* forward: 5′ GTTTAATTCGATGATACGCGAG 3′
> *Bacteroidetes* reverse: 5′ TTAACCCGACACCTCACGG 3′
> *Eubacteria* forward: 5′ ACTCCTACGGGAGGCAGCAGT 3′
> *Eubacteria* reverse: 5′ ATTACCGCGGCTGCTGGC 3′

10. Histological evaluation

The histological examination was conducted using optical microscopy by an independent histologist who was blinded to the experimental groups. Samples from the duodenum, jejunum, and ileum were fixed, dehydrated in ethanol, embedded in paraffin wax, and sectioned using a microtome (Reichert). The resulting 5-micron sections were stained with hematoxylin and eosin, as well as periodic acid-Schiff stain, to assess goblet cells and mucus secretion. Quantification was carried out in a high-power field, examining 20 fields at ×400 magnification for each animal using a computerized image analyzer (Image Pro Plus, Media Cybernetics Corp). A semiquantitative score was used for microscopic evaluation.[25] Additionally, the same operator performed both qualitative analysis and structural description, focusing on the following parameters: villous architecture, localization of chronic inflammatory infiltrate, lymphocyte accumulation, presence or absence of lymphangiectasia, and characteristics of Brunner's glands in duodenum samples.

11. Statistical analysis

Data are presented as mean ± standard deviation or median (range) depending on whether the distribution is normal or skewed, respectively. Differences between groups were assessed using the unpaired Student *t*-test or the Mann-Whitney *U*-test based on the distribution of the data. To determine correlations between parameters, Pearson or Spearman analyses were employed for parametric or nonparametric variables, respectively. Statistical analyses were conducted using the SPSS 19.0 software package (IBM Corp.) and GraphPad Prism 5.01 software (GraphPad Software); a *p*-value of less than 0.05 was considered statistically significant.

RESULTS

Table 1 demonstrates that, as anticipated, rats fed a hypercaloric diet experienced significantly greater weight gain compared to the control group at the conclusion of the study. Additionally, VAT, liver and gut weight, and total fat mass were higher in the HFSD group than in the control group ($p<0.05$). The HFSD group also exhibited increased fat accumulation in duodenal tissue (0.55±0.10 vs 0.45±0.09 g/g, $p=0.024$). Caloric intake was

Table 1. Anthropometric and metabolic parameters, daily calorie intake and lipid profile of control and HFSD groups

Parameter	Control (n=10)	HFSD (n=10)	*p*-value
Weight gain (g)	249±37	290±35	0.037
Total calorie intake (kcal/100 g/day)	15 (13–28)	23 (17–43)	<0.0001
Body fat content (g)	13.3 (9.5–19.1)	23.9 (13.9–52.3)	<0.0001
Visceral adipose tissue weight (g)	5.3 (4.1–8.1)	8.6 (4.7–19.2)	0.0026
Liver weight (g)	15.0 (8.7–18.4)	17.2 (13.4–23.1)	0.004
Gut weight (g)	12.2±1.9	10.5±1.3	0.011
CIF (g/g tissue)	0.45±0.09	0.55±0.10	0.024
Glucose (mg/dL)	141±12	163±13	0.001
TC (mg/dL)	59±10	60±7	NS
HDL-C (mg/dL)	41±4	39±4	NS
Non-HDL-C (mg/dL)	15±6	22±3	0.004
TG (mg/dL)	76 (40–146)	160 (44–325)	<0.0001
TG/HDL-C	1.5 (1.1–3.0)	6.1 (2.9–7.7)	<0.0001
FFA (mmol/L)	0.51±0.12	0.66±0.16	0.015

Results are expressed as mean ± standard deviation or median (range) for skewed distributed data. Student *t*-test or Mann-Whitney *U*-test, respectively.
HFSD, high fat and sucrose diet; CIF, cell intestinal fat; TC, total cholesterol; HDL-C, high-density lipoprotein cholesterol; TG, triglycerides; FFA, free fatty acid; NS, not significant.

higher in HFSD rats as well. The HFSD group showed elevated levels of plasma TG (p=0.05), non-HDL-C (non-HDL-C) (p=0.011), FFA (p=0.015), glucose (p=0.003), and the TG/HDL-C index (p<0.0001). However, no significant differences were observed in total cholesterol or HDL-C levels. Additionally, the HFSD group had higher serum levels of LPS (p=0.016) (**Fig. 1A**) and an increased F/B ratio compared to the control group, indicating an altered microbiota (p=0.022) (**Fig. 1B**).
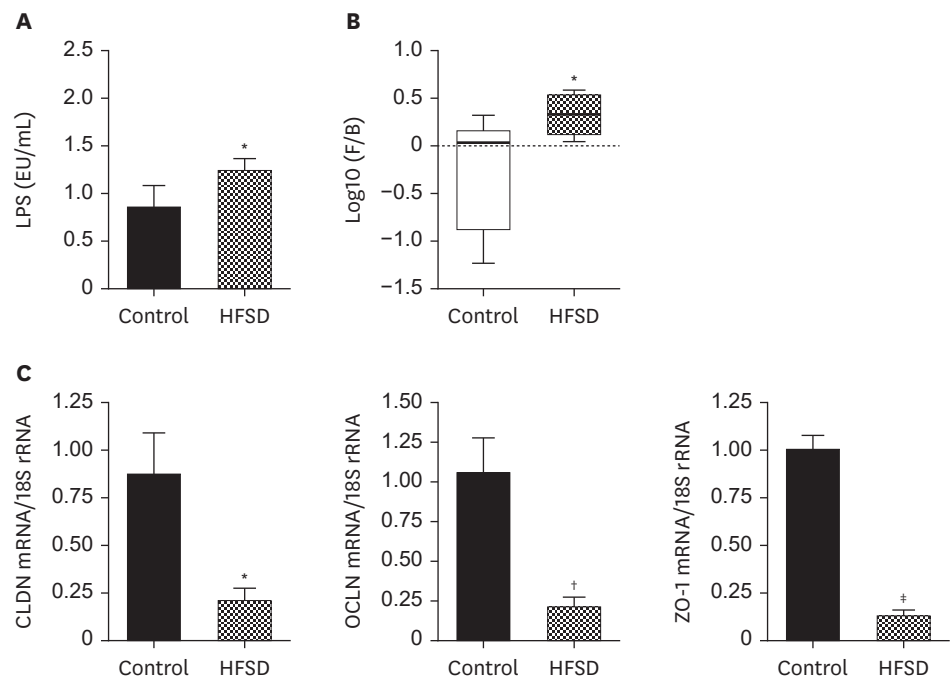
Fig. 1. Intestinal integrity and dysbiosis evaluation. Results are expressed as mean ± standard deviation. The Student *t*-test was performed: (A) *p=0.016 vs. control. (B) *p=0.022 vs. control. (C) *p=0.0016 vs. control; †p<0.001 vs. control; ‡p=0.0095 vs. control.
HFSD, high fat and sucrose diet; LPS, lipopolysaccharides; EU, endotoxin units; F, *Firmicutes*; B, *Bacteroidetes*; CLDN, claudin; OCLN, occludin; ZO-1, zonula occludens 1.

Table 2. Lipid composition of chylomicron isolated from control and HFSD groups

Parameter	Control (n=10)	HFSD (n=10)	*p*-value
Total cholesterol (mg/dL)	5±2	7±2	NS
TG (mg/dL)	37±8	181±43	0.010
Cholesterol/TG (mg/dL)	0.10±0.05	0.07±0.02	NS
PL (mg/dL)	1.14±0.18	2.86±1.15	0.007
LPS (EU/mL)	2.07±1.15	8.58±4.55	0.004

Results are expressed as mean ± standard deviation. Student *t*-test was performed.
HFSD, high fat and sucrose diet; TG, triglycerides; PL, phospholipids; LPS, lipopolysaccharides; EU, endotoxin units; NS, not significant.

When evaluating gut integrity, the HFSD group exhibited lower expression levels of claudin (HFSD: 0.13±0.07 RU vs. control: 1.01±0.12 RU, *p*=0.0016), occludin (HFSD: 0.21±0.16 RU vs. control: 1.07±0.38 RU, *p*<0.001), and zonula occludens-1 (HFSD: 0.27±0.10 RU vs. control: 0.88±0.37 RU, *p*=0.0095) compared to the control group (**Fig. 1C**).

Furthermore, the histological examination of the intestine did not reveal significant differences in any of its segments based on the semiquantitative score used (*p*>0.05). However, a comparison between the HFSD and control groups showed altered villous architecture and a significantly increased accumulation of lymphocytes in the ileum wall (*p*=0.019). This change corresponds to the gradient of the chronic inflammatory process observed from the duodenum to the distal ileum (**Fig. 2**).

Table 2 presents the composition of isolated CM lipids. CMs from HFSD rats exhibited an almost 5-fold increase in TG (*p*=0.010), more than double the PL (*p*=0.007), and higher LPS content compared to the control group (*p*=0.004). LPS levels showed a positive correlation with CM-TG content (r=0.74, *p*<0.05) and non-HDL-C (r=0.77, *p*<0.05).

ApoB mRNA levels did not differ significantly between the control and HFSD rats, despite a 30% increase (control: 1.14±0.61 RU vs HFSD: 1.36±1.31 RU, *p*=0.712).

Regarding MTTP expression in duodenal tissue, an increase was observed with HFSD (HFSD: 1.28 ± 0.65 RU vs C: 0.79 ± 0.42 RU, *p*=0.027). This increase directly correlated with CM-TG (r=0.53, *p*=0.036) and inversely with CIF (r=-0.6357, *p*=0.0356) (**Fig. 3**).

DISCUSSION

In the present study, we evaluated the chemical composition of CMs, their association with MTTP expression, potential intestinal fat depots, and alterations in gut integrity and inflammation within a diet-induced dysbiosis animal model. In animals fed an HFSD, we observed a state of dysbiosis and an altered lipid profile indicative of IR. Additionally, HFSD rats exhibited an over-enrichment of TG in CM particles, concurrent with increases in gut fat storage, gut permeability, and circulating LPS levels. To our knowledge, this is the first study to assess the chemical characteristics of CM in relation to MTTP in a model of IR and dysbiosis.

One of the most important factors affecting the state of the microbiota is undoubtedly diet.[26] There is strong evidence that the Western diet, which is high in both saturated fats and sugar, disrupts the microbiota,[14,27,28] intensifies chronic inflammation, and consequently leads to the development of metabolic disorders such as IR, obesity, type 2 diabetes, and cardiovascular diseases.[13,14] Alterations in the GM due to an HFSD result in an increased proportion of LPS-
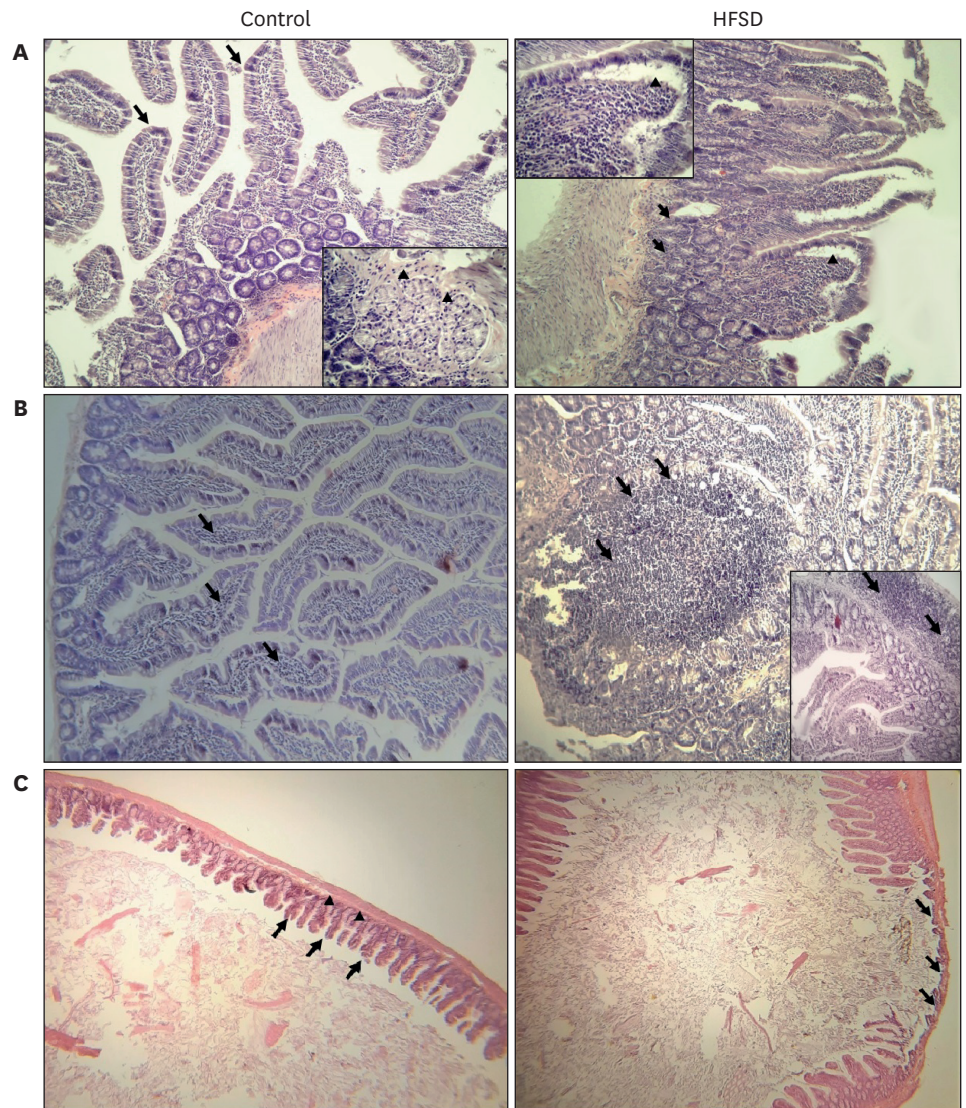
Fig. 2. Histological images of duodenum (A), jejunum (B), and ileum (C) of the control and HFSD group. Representative histological duodenum section from Control and HFSD groups with hematoxylin and eosin staining (×40). (A) Control: preserved villous architecture (black arrows, ×40) and Brunner´s gland (black arrowheads, detail ×100). HFSD: altered villous architecture with a predominant chronic inflammatory infiltrate distributed in the villi (black arrowheads, detail ×100). Vascular congestion and lymphocytic accumulation in lamina propria (black arrows, ×40). Cryptic epithelium with mild reactive changes. Shortened and widened villi (black arrowheads, detail ×40). (B) Control: preserved villous architecture (black arrows). Cryptic epithelium without significant histological alterations. HFSD: significant chorion chronic inflammatory infiltrate with eosinophils and expansive lymphocyte accumulation and vascular congestion (black arrows). (C) Control: preserved villous architecture (black arrows). Cryptic epithelium without significant histological alterations. HFSD: Lamina propria section with discrete wall chronic inflammatory infiltrates and vascular congestion. Thinned wall with section loss villous (black arrows). HFSD, high fat and sucrose diet.

containing microbiota in the gut, which is associated with increased glycemia and insulinemia.[13] In fact, the results observed in the HFSD model were as expected, with an increase in circulating LPS levels indicating higher intestinal permeability, a characteristic of dysbiosis. This was also associated with reduced expression of gut TJ proteins and the development of an IR state.[29-32] This metabolic and dysbiotic state is likely accompanied by changes in the composition of the microbiota, although this was not specifically determined in this study. Instead, we measured
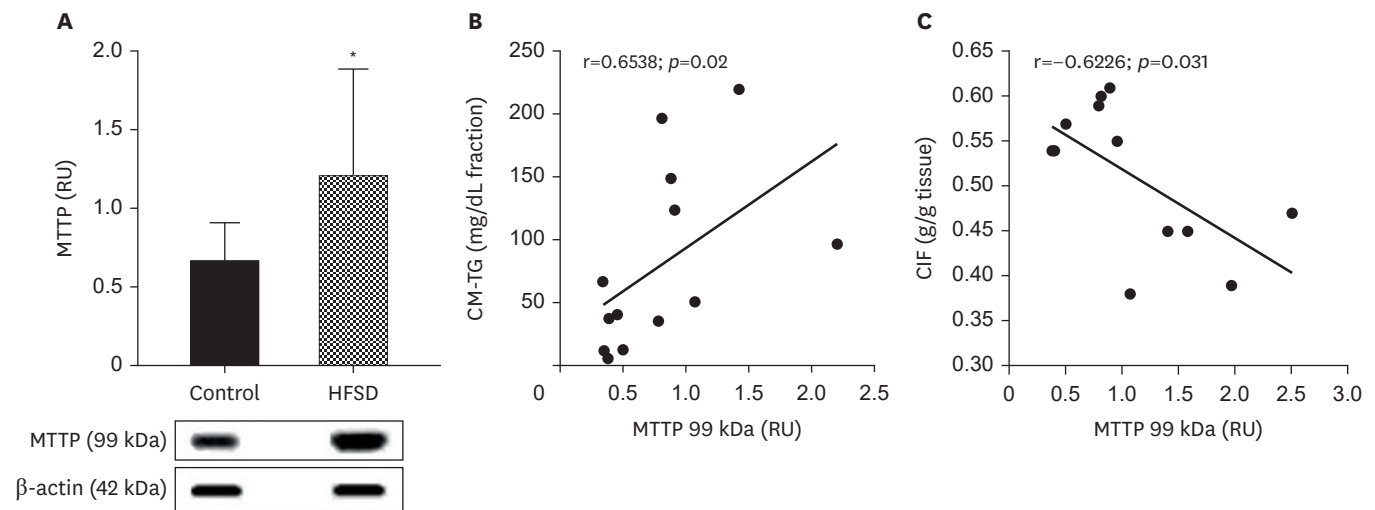
Fig. 3. Duodenal expression of MTTP in the control and HFSD groups (A) and the associations of MTTP with CM-TG (B), and CIF (C). Results are expressed as mean ± standard deviation. (A) Student t-test: *$p<0.05$ vs. control. (B, C) Pearson correlations.
MTTP, microsomal triglyceride transfer protein; RU, relative units; HFSD, high rat and sucrose diet; CM-TG, chylomicron triglycerides; CIF, cell intestinal fat.

the widely used F/B ratio as an estimator of microbiota imbalance, which was found to be increased in the HFSD group, consistent with a state of dysbiosis.[33]

HFSD rats constitute an adequate pathophysiological model not only for IR but also for dysbiosis, due to their dietary adaptability and the rapid development of metabolic disorders in short-term studies. Dysbiosis is linked to numerous systemic and local abnormalities, notably the disruption of the gut barrier.[28] The intestinal barrier is a complex structure that includes the GM, a mucus layer, a monolayer of epithelial cells, and immune cells located in the lamina propria and submucosa.[34,35] Numerous studies have documented the relationship between alterations in the microbiota due to an HFD and increased gut barrier permeability.[36-38] In our study, we noted a disruption in the normal structure of the intestine and a decreased expression of genes encoding TJ proteins, accompanied by an increase in serum LPS levels. These findings suggest a compromise in intestinal integrity in this model of IR and HFSD-induced dysbiosis.

LPS contains lipid A, which can cross the intestinal mucosa with the aid of CMs.[38] In this scenario, lipoproteins may trigger an inflammatory response in tissues such as the liver and adipose tissue, leading to an IR state typically associated with obesity.[39,40] In adipose tissue, the interaction between LPS and LPS binding protein can activate the CD14 receptor. This complex then binds to Toll-like receptor 4 on macrophages and adipose cells, promoting the expression of genes that encode pro-inflammatory proteins.[40]

Regarding the metabolic and lipid profile, the group receiving a pro-dysbiotic diet exhibited a harmful and pro-atherogenic lipid and metabolic profile, associated with IR status. One of the strengths of our study was the isolation of the CMs. These particles are challenging to isolate due to their physical characteristics, including heterogeneous size and composition,[41] and have not yet been evaluated in this HFSD-induced IR and dysbiosis model. CM particles from the HFSD group showed higher TG content than controls, directly associated with LPS levels, suggesting that altered microbiota could modulate the composition of CMs. These findings align with those of Clemente-Postigo et al., who noted that morbidly obese

patients with postprandial hypertriglyceridemia exhibited a significant increase in LPS levels in serum and the CM fraction following a fat overload.[31] TG-enriched CMs could serve as a better substrate for LPL, releasing oxidative and harmful FAs, and promoting the production of smaller rCMs, which could more easily penetrate the subendothelium and promote the atherosclerotic process.[3]

Concerning intestinal apoB levels, although several studies have demonstrated an increase in the expression of intestinal apoB48 in animal models of IR and type 2 diabetes, which is associated with the overproduction of apoB48-containing lipoproteins,[42-44] our study did not observe any significant differences in intestinal apoB mRNA levels between groups. Given that the quantity of apoB48 is a limiting factor for CM assembly in the intestine,[15] these findings imply that despite higher intestinal TG levels and increased MTTP levels, there is not necessarily an increase in the number of secreted particles, but rather an increase in their TG content and size. Considering that other factors also regulate apoB *in vivo*, these discrepancies could be partially attributed to differences in species and experimental models used.

MTTP catalyzes the assembly of TG, cholesteryl esters, and PL with apoB48 to form primordial CMs. These CMs can then undergo lipidation to become pre-CMs or be stored in enterocytes depending on the availability of apoB48.[45,46] The expression of MTTP is influenced by diet, particularly the amount and composition of lipids. Hamsters on an HFD exhibit increased intestinal MTTP protein expression compared to those on high sucrose diets, where no increase is observed. It is important to note that MTTP is negatively regulated by insulin, and higher expression levels of MTTP have been observed in insulin-resistant states.[47,48] As previously mentioned, increased MTTP expression is associated with enhanced secretion of TG-rich lipoproteins (TRLs).[49,50] However, the impact of MTTP protein expression on CM lipid composition has been minimally explored. Additionally, animal models deficient in MTTP, whether on a Western diet or not, have shown lipid accumulation in intestinal depots.[51,52]

Until now, the relationship between the expression and activity of MTTP in IR animal models has not been extensively explored. Our findings indicate an increased expression of MTTP in HFSD, aligning with previous studies on HFD[53] and IR.[54] In our research, using a model of IR and dysbiosis induced by diet, both factors could account for these observations. Additionally, MTTP expression was linked to the production of TG-enriched CM and CIF. These findings imply that within the metabolic framework of IR accompanied by intestinal dysbiosis, MTTP facilitates the secretion of CM particles that are excessively rich in TG, leading to increased fat deposition in the intestine.

We acknowledge several limitations in this study. First, lipoprotein size, a key determinant of atherogenic potential, was not assessed.[55] Second, additional components of the particle, such as apoCIII or apoE, which contribute to the retention of remnants in the subendothelium, as well as certain highly inflammatory types of fatty acids, could have provided further insights into the atherogenic potential of the lipoproteins studied. Third, the TRL fraction analyzed in this research may not have been composed solely of CMs, but also of large VLDL. Given this limitation, and the challenges associated with purifying CMs through ultracentrifugation, we refer to the lipoprotein fraction we analyzed as the "CM-enriched fraction." Fourth, although the Syrian golden hamster is considered the optimal model for assessing CM metabolism due to its significant similarity to humans,[44] HFSD rats still serve as a viable model for studying TRL metabolism and for extrapolating findings to humans.

In conclusion, our findings are consistent with a model suggesting that gut dysbiosis and the development of IR are linked, where intestinal TG content plays a crucial role in the secretion of TG-rich CMs. This process is facilitated by MTTP and is associated with an increased atherogenic potential.

REFERENCES

1. Wolska A, Dunbar RL, Freeman LA, Ueda M, Amar MJ, Sviridov DO, et al. Apolipoprotein C-II: new findings related to genetics, biochemistry, and role in triglyceride metabolism. Atherosclerosis 2017;267:49-60. **PUBMED** | **CROSSREF**

2. Dash S, Xiao C, Morgantini C, Lewis GF. New insights into the regulation of chylomicron production. Annu Rev Nutr 2015;35:265-294. **PUBMED** | **CROSSREF**

3. Ginsberg HN, Packard CJ, Chapman MJ, Borén J, Aguilar-Salinas CA, Averna M, et al. Triglyceride-rich lipoproteins and their remnants: metabolic insights, role in atherosclerotic cardiovascular disease, and emerging therapeutic strategies-a consensus statement from the European Atherosclerosis Society. Eur Heart J 2021;42:4791-4806. **PUBMED** | **CROSSREF**

4. Masuda D, Yamashita S. Postprandial hyperlipidemia and remnant lipoproteins. J Atheroscler Thromb 2017;24:95-109. **PUBMED** | **CROSSREF**

5. Duran EK, Pradhan AD. Triglyceride-rich lipoprotein remnants and cardiovascular disease. Clin Chem 2021;67:183-196. **PUBMED** | **CROSSREF**

6. Zago V, Lucero D, Macri EV, Cacciagiú L, Gamba CA, Miksztowicz V, et al. Circulating very-low-density lipoprotein characteristics resulting from fatty liver in an insulin resistance rat model. Ann Nutr Metab 2010;56:198-206. **PUBMED** | **CROSSREF**

7. Lucero D, López GI, Gorzalczany S, Duarte M, González Ballerga E, Sordá J, et al. Alterations in triglyceride rich lipoproteins are related to endothelial dysfunction in metabolic syndrome. Clin Biochem 2016;49:932-935. **PUBMED** | **CROSSREF**

8. Adak A, Khan MR. An insight into gut microbiota and its functionalities. Cell Mol Life Sci 2019;76:473-493. **PUBMED** | **CROSSREF**

9. Araújo JR, Tomas J, Brenner C, Sansonetti PJ. Impact of high-fat diet on the intestinal microbiota and small intestinal physiology before and after the onset of obesity. Biochimie 2017;141:97-106. **PUBMED** | **CROSSREF**

10. Dabke K, Hendrick G, Devkota S. The gut microbiome and metabolic syndrome. J Clin Invest 2019;129:4050-4057. **PUBMED** | **CROSSREF**

11. Matey-Hernandez ML, Williams FMK, Potter T, Valdes AM, Spector TD, Menni C. Genetic and microbiome influence on lipid metabolism and dyslipidemia. Physiol Genomics 2018;50:117-126. **PUBMED** | **CROSSREF**

12. Allam-Ndoul B, Castonguay-Paradis S, Veilleux A. Gut microbiota and intestinal trans-epithelial permeability. Int J Mol Sci 2020;21:6402. **PUBMED** | **CROSSREF**

13. Cani PD, Amar J, Iglesias MA, Poggi M, Knauf C, Bastelica D, et al. Metabolic endotoxemia initiates obesity and insulin resistance. Diabetes 2007;56:1761-1772. **PUBMED** | **CROSSREF**

14. Cani PD, Bibiloni R, Knauf C, Waget A, Neyrinck AM, Delzenne NM, et al. Changes in gut microbiota control metabolic endotoxemia-induced inflammation in high-fat diet-induced obesity and diabetes in mice. Diabetes 2008;57:1470-1481. **PUBMED** | **CROSSREF**

15. Giammanco A, Cefalù AB, Noto D, Averna MR. The pathophysiology of intestinal lipoprotein production. Front Physiol 2015;6:61. **PUBMED** | **CROSSREF**

16. Hussain MM, Rava P, Walsh M, Rana M, Iqbal J. Multiple functions of microsomal triglyceride transfer protein. Nutr Metab (Lond) 2012;9:14. **PUBMED** | **CROSSREF**

17. Berriot-Varoqueaux N, Aggerbeck LP, Samson-Bouma M, Wetterau JR. The role of the microsomal triglygeride transfer protein in abetalipoproteinemia. Annu Rev Nutr 2000;20:663-697. **PUBMED** | **CROSSREF**

18. Shoulders CC, Brett DJ, Bayliss JD, Narcisi TM, Jarmuz A, Grantham TT, et al. Abetalipoproteinemia is caused by defects of the gene encoding the 97 kDa subunit of a microsomal triglyceride transfer protein. Hum Mol Genet 1993;2:2109-2116. **PUBMED** | **CROSSREF**

19. Xie Y, Matsumoto H, Kennedy S, Newberry EP, Moritz W, DeBosch BJ, et al. Impaired chylomicron assembly modifies hepatic metabolism through bile acid dependent and transmissible microbial adaptations. Hepatology 2019;70:1168-1184. **PUBMED** | **CROSSREF**

20. Fiske CH, Subbarow Y. The colorimetric determination of phosphorus. J Biol Chem 1925;66:375-400.
    CROSSREF

21. Folch J, Lees M, Sloane Stanley GH. A simple method for the isolation and purification of total lipides from animal tissues. J Biol Chem 1957;226:497-509.   PUBMED | CROSSREF

22. Repetto EM, Wiszniewski M, Bonelli AL, Vecino CV, Martinez Calejman C, Arias P, et al. Impaired HPA axis function in diabetes involves adrenal apoptosis and phagocytosis. Endocrine 2019;63:602-614.
    PUBMED | CROSSREF

23. Pfaffl MW. A new mathematical model for relative quantification in real-time RT-PCR. Nucleic Acids Res 2001;29:e45.   PUBMED | CROSSREF

24. Lowry OH, Rosebrough NJ, Farr AL, Randall RJ. Protein measurement with the Folin phenol reagent. J Biol Chem 1951;193:265-275.   PUBMED | CROSSREF

25. Cattaruzza F, Cenac N, Barocelli E, Impicciatore M, Hyun E, Vergnolle N, et al. Protective effect of proteinase-activated receptor 2 activation on motility impairment and tissue damage induced by intestinal ischemia/reperfusion in rodents. Am J Pathol 2006;169:177-188.   PUBMED | CROSSREF

26. Moszak M, Szulińska M, Bogdański P. You are what you eat-the relationship between diet, microbiota, and metabolic disorders-a review. Nutrients 2020;12:1096.   PUBMED | CROSSREF

27. Turnbaugh PJ, Backhed F, Fulton L, Gordon JI. Marked alterations in the distal gut microbiome linked to diet induced obesity. Cell Host Microbe 2008;3:213-223.   PUBMED | CROSSREF

28. Malesza IJ, Malesza M, Walkowiak J, Mussin N, Walkowiak D, Aringazina R, et al. High-fat, western-style diet, systemic inflammation, and gut microbiota: a narrative review. Cells 2021;10:3164.   PUBMED | CROSSREF

29. Feng Y, Huang Y, Wang Y, Wang P, Song H, Wang F. Antibiotics induced intestinal tight junction barrier dysfunction is associated with microbiota dysbiosis, activated NLRP3 inflammasome and autophagy. PLoS One 2019;14:e0218384.   PUBMED | CROSSREF

30. Nakanishi T, Fukui H, Wang X, Nishiumi S, Yokota H, Makizaki Y, et al. Effect of a high-fat diet on the small-intestinal environment and mucosal integrity in the gut-liver axis. Cells 2021;10:3168.   PUBMED | CROSSREF

31. Clemente-Postigo M, Queipo-Ortuño MI, Murri M, Boto-Ordoñez M, Perez-Martinez P, Andres-Lacueva C, et al. Endotoxin increase after fat overload is related to postprandial hypertriglyceridemia in morbidly obese patients. J Lipid Res 2012;53:973-978.   PUBMED | CROSSREF

32. Boulangé CL, Neves AL, Chilloux J, Nicholson JK, Dumas ME. Impact of the gut microbiota on inflammation, obesity, and metabolic disease. Genome Med 2016;8:42.   PUBMED | CROSSREF

33. Ley RE, Turnbaugh PJ, Klein S, Gordon JI. Microbial ecology: human gut microbes associated with obesity. Nature 2006;444:1022-1023.   PUBMED | CROSSREF

34. Di Tommaso N, Gasbarrini A, Ponziani FR. Intestinal barrier in human health and disease. Int J Environ Res Public Health 2021;18:12836.   PUBMED | CROSSREF

35. Martel J, Chang SH, Ko YF, Hwang TL, Young JD, Ojcius DM. Gut barrier disruption and chronic disease. Trends Endocrinol Metab 2022;33:247-265.   PUBMED | CROSSREF

36. Lam YY, Ha CWY, Hoffmann JMA, Oscarsson J, Dinudom A, Mather TJ, et al. Effects of dietary fat profile on gut permeability and microbiota and their relationships with metabolic changes in mice. Obesity (Silver Spring) 2015;23:1429-1439.   PUBMED | CROSSREF

37. Kim SJ, Kim SE, Kim AR, Kang S, Park MY, Sung MK. Dietary fat intake and age modulate the composition of the gut microbiota and colonic inflammation in C57BL/6J mice. BMC Microbiol 2019;19:193.   PUBMED | CROSSREF

38. Ghoshal S, Witta J, Zhong J, de Villiers W, Eckhardt E. Chylomicrons promote intestinal absorption of lipopolysaccharides. J Lipid Res 2009;50:90-97.   PUBMED | CROSSREF

39. Rivera CA, Gaskin L, Singer G, Houghton J, Allman M. Western diet enhances hepatic inflammation in mice exposed to cecal ligation and puncture. BMC Physiol 2010;10:20.   PUBMED | CROSSREF

40. Guo S, Nighot M, Al-Sadi R, Alhmoud T, Nighot P, Ma TY. Lipopolysaccharide regulation of intestinal tight junction permeability is mediated by TLR-4 signal transduction pathway activation of FAK and MyD88. J Immunol 2015;195:4999-5010.   PUBMED | CROSSREF

41. Hidaka H, Tozuka M, Meyer B, Yamauchi K, Sugano M, Nakabayashi T, et al. Characterization of triglyceride rich lipoproteins with very light density by ultracentrifugation and agarose gel electrophoresis using triglyceride- and cholesterol-staining. Ann Clin Lab Sci 2003;33:167-178.   PUBMED

42. Haidari M, Leung N, Mahbub F, Uffelman KD, Kohen-Avramoglu R, Lewis GF, et al. Fasting and postprandial overproduction of intestinally derived lipoproteins in an animal model of insulin resistance. Evidence that chronic fructose feeding in the hamster is accompanied by enhanced intestinal de novo

lipogenesis and ApoB48-containing lipoprotein overproduction. J Biol Chem 2002;277:31646-31655.
PUBMED | **CROSSREF**

43. Zoltowska M, Ziv E, Delvin E, Sinnett D, Kalman R, Garofalo C, et al. Cellular aspects of intestinal lipoprotein assembly in Psammomys obesus: a model of insulin resistance and type 2 diabetes. Diabetes 2003;52:2539-2545. **PUBMED** | **CROSSREF**

44. Lally S, Owens D, Tomkin GH. The different effect of pioglitazone as compared to insulin on expression of hepatic and intestinal genes regulating post-prandial lipoproteins in diabetes. Atherosclerosis 2007;193:343-351. **PUBMED** | **CROSSREF**

45. Pan X, Hussain MM. Gut triglyceride production. Biochim Biophys Acta 2012;1821:727-735. **PUBMED** | **CROSSREF**

46. Xiao C, Stahel P, Lewis GF. Regulation of chylomicron secretion: focus on post-assembly mechanisms. Cell Mol Gastroenterol Hepatol 2019;7:487-501. **PUBMED** | **CROSSREF**

47. Hussain MM, Nijstad N, Franceschini L. Regulation of microsomal triglyceride transfer protein. Clin Lipidol 2011;6:293-303. **PUBMED** | **CROSSREF**

48. Lin X, Ma P, Yang C, Wang J, He K, Chen G, et al. Dietary-induced elevations of triglyceride-rich lipoproteins promote atherosclerosis in the low-density lipoprotein receptor knockout Syrian golden hamster. Front Cardiovasc Med 2021;8:738060. **PUBMED** | **CROSSREF**

49. Gleeson A, Anderton K, Owens D, Bennett A, Collins P, Johnson A, et al. The role of microsomal triglyceride transfer protein and dietary cholesterol in chylomicron production in diabetes. Diabetologia 1999;42:944-948. **PUBMED** | **CROSSREF**

50. Sirwi A, Hussain MM. Lipid transfer proteins in the assembly of apoB-containing lipoproteins. J Lipid Res 2018;59:1094-1102. **PUBMED** | **CROSSREF**

51. Xie Y, Newberry EP, Young SG, Robine S, Hamilton RL, Wong JS, et al. Compensatory increase in hepatic lipogenesis in mice with conditional intestine-specific Mttp deficiency. J Biol Chem 2006;281:4075-4086. **PUBMED** | **CROSSREF**

52. Iqbal J, Parks JS, Hussain MM. Lipid absorption defects in intestine-specific microsomal triglyceride transfer protein and ATP-binding cassette transporter A1-deficient mice. J Biol Chem 2013;288:30432-30444. **PUBMED** | **CROSSREF**

53. Graulet B, Gruffat D, Durand D, Bauchart D. Small intestine and liver microsomal triacylglycerol transfer protein in the bovine and rat: effects of dietary coconut oil. J Dairy Sci 2004;87:3858-3868. **PUBMED** | **CROSSREF**

54. Phillips C, Owens D, Collins P, Tomkin GH. Microsomal triglyceride transfer protein: does insulin resistance play a role in the regulation of chylomicron assembly? Atherosclerosis 2002;160:355-360. **PUBMED** | **CROSSREF**

55. Libby P, Buring JE, Badimon L, Hansson GK, Deanfield J, Bittencourt MS, et al. Atherosclerosis. Nat Rev Dis Primers 2019;5:56. **PUBMED** | **CROSSREF**